Journal of Zhejiang University-SCIENCE B (Biomedicine & Biotechnology) *2024 25(10):857-877*
www.jzus.zju.edu.cn; www.springer.com/journal/11585
E-mail: jzus_b@zju.edu.cn

Review

https://doi.org/10.1631/jzus.B2300401

Check for updates

Aberrant dynamic functional connectivity of thalamocortical circuitry in major depressive disorder

Weihao ZHENG[1], Qin ZHANG[1], Ziyang ZHAO[1], Pengfei ZHANG[2,3,4], Leilei ZHAO[1], Xiaomin WANG[1], Songyu YANG[1], Jing ZHANG[2,3,4]✉, Zhijun YAO[1]✉, Bin HU[1,5,6,7]✉

[1]*Gansu Provincial Key Laboratory of Wearable Computing, School of Information Science and Engineering, Lanzhou University, Lanzhou 730000, China*
[2]*Second Clinical School, Lanzhou University, Lanzhou 730030, China*
[3]*Department of Magnetic Resonance, Lanzhou University Second Hospital, Lanzhou 730030, China*
[4]*Gansu Province Clinical Research Center for Functional and Molecular Imaging, Lanzhou 730030, China*
[5]*School of Medical Technology, Beijing Institute of Technology, Beijing 100081, China*
[6]*CAS Center for Excellence in Brain Science and Intelligence Technology, Shanghai Institutes for Biological Sciences, Chinese Academy of Sciences, Shanghai 200031, China*
[7]*Joint Research Center for Cognitive Neurosensor Technology of Lanzhou University & Institute of Semiconductors, Chinese Academy of Sciences, Lanzhou 730000, China*

Abstract: Thalamocortical circuitry has a substantial impact on emotion and cognition. Previous studies have demonstrated alterations in thalamocortical functional connectivity (FC), characterized by region-dependent hypo- or hyper-connectivity, among individuals with major depressive disorder (MDD). However, the dynamical reconfiguration of the thalamocortical system over time and potential abnormalities in dynamic thalamocortical connectivity associated with MDD remain unclear. Hence, we analyzed dynamic FC (dFC) between ten thalamic subregions and seven cortical subnetworks from resting-state functional magnetic resonance images of 48 patients with MDD and 57 healthy controls (HCs) to investigate time-varying changes in thalamocortical FC in patients with MDD. Moreover, dynamic laterality analysis was conducted to examine the changes in functional lateralization of the thalamocortical system over time. Correlations between the dynamic measures of thalamocortical FC and clinical assessment were also calculated. We identified four dynamic states of thalamocortical circuitry wherein patients with MDD exhibited decreased fractional time and reduced transitions within a negative connectivity state that showed strong correlations with primary cortical networks, compared with the HCs. In addition, MDD patients also exhibited increased fluctuations in functional laterality in the thalamocortical system across the scan duration. The thalamo-subnetwork analysis unveiled abnormal dFC variability involving higher-order cortical networks in the MDD cohort. Significant correlations were found between increased dFC variability with dorsal attention and default mode networks and the severity of symptoms. Our study comprehensively investigated the pattern of alteration of the thalamocortical dFC in MDD patients. The heterogeneous alterations of dFC between the thalamus and both primary and higher-order cortical networks may help characterize the deficits of sensory and cognitive processing in MDD.

Key words: Major depressive disorder; Resting-state functional magnetic resonance imaging; Thalamocortical circuitry; Dynamic functional connectivity; Dynamic laterality

1 Introduction

Major depressive disorder (MDD) is a prevalent psychiatric disorder characterized by persistent depression, anhedonia, and cognitive function impairment (Otte et al., 2016). It is associated with atypical brain activity and functional interactions within large-scale brain networks (Kaiser et al., 2015; Sacchet et al., 2016; Zhao et al., 2022). The thalamus, known for its

✉ Bin HU, bh@lzu.edu.cn
Zhijun YAO, yaozj@lzu.edu.cn
Jing ZHANG, ery_zhangjing@lzu.edu.cn
Bin HU, https://orcid.org/0000-0003-3514-5413
Zhijun YAO, https://orcid.org/0000-0003-0057-0831
Jing ZHANG, https://orcid.org/0000-0002-1678-5688

Received June 5, 2023; Revision accepted Sept. 24, 2023;
Crosschecked Feb. 1, 2024; Published online Feb. 24, 2024

intricate feedforward and feedback connections with the cortex, has been implicated in the transmission and regulation of information between cortical regions (Sherman, 2007). A previous study by Yuan et al. (2016) indicated that the dysfunctional circuits involving the thalamus may contribute to the clinical symptoms and cognitive impairments of MDD. Therefore, investigating brain network dysfunctions in patients with MDD requires a comprehensive examination of thalamic involvement (Behrens et al., 2003; Zhang et al., 2010), and exploring thalamocortical connectivity may offer further insights into the pathogenesis and pathophysiological process of MDD.

Resting-state functional magnetic resonance imaging (rs-fMRI) provides an effective approach to systematically investigate thalamocortical circuitry by estimating functional connectivity (FC). Several studies have found an association between altered thalamocortical FC and MDD, suggesting that disrupted thalamocortical FC may serve as a neurobiological marker for MDD (Brown et al., 2017; Kong et al., 2018). For example, Lui et al. (2011) reported an association between decreased thalamo-prefrontal connectivity and treatment resistance in patients with depression. Additionally, reduced FC between the thalamus and bilateral precuneus after electroconvulsive therapy adversely affects cognitive performance in individuals with MDD (Wei et al., 2020). Moreover, MDD patients have demonstrated decreased connectivity between the thalamus and the orbitofrontal cortex (Tadayonnejad et al., 2015), along with increased connectivity connecting the thalamus to the temporal (Brown et al., 2017) and somatosensory cortices (Kang et al., 2018). Nevertheless, these studies assumed the constancy of brain connectivity patterns during the entire scan, overlooking the dynamic nature of the brain.

Previous studies have revealed that the brain operates as a dynamic system, and the resting-state FC can vary across different temporal scales (Hutchison et al., 2013; Allen et al., 2014). To capture the temporal variability of FC and uncover underlying neurophysiological mechanisms that static FC analysis fails to detect, the concept of dynamic FC (dFC) analysis was introduced (Allen et al., 2014). Recent studies using the sliding-window method have identified dFC dysconnectivity within and between resting-state connectivity networks in patients with MDD, suggesting a potential connection between the dFC properties and cognitive performance and the severity of depression (Zhi et al., 2018; Yao et al., 2019a; Sendi et al., 2021). Moreover, individuals with MDD and bipolar depression exhibited shared and distinct disruptions in thalamocortical dFC variability, further substantiating the significance of thalamocortical FC dynamics in the pathological mechanism underlying depression (Lu et al., 2023). However, there have been few investigations into thalamocortical dFC patterns in MDD, and the sliding-window method fails to capture sudden changes in FC patterns effectively (Lindquist et al., 2014). In contrast, the dynamic conditional correlation (DCC) model estimates FC at each time point by considering time courses as a weighted combination of preceding time points, demonstrating superior performance compared to the sliding-window method (Lindquist et al., 2014; Choe et al., 2017). Nevertheless, the DCC model assumes zero autocorrelation among the input samples, which may not always hold (Lenoski et al., 2008; Arbabshirani et al., 2014). To address this issue, an auto-regressive DCC (AR-DCC) model was proposed, which better captures the dFC patterns in the brain compared with both the sliding-window method and the DCC model (Hakimdavoodi and Amirmazlaghani, 2020). By using the AR-DCC model, researchers have reported altered dFC in the frontoparietal, dorsal attention, and sensorimotor networks in patients with attention-deficit/hyperactivity disorder (ADHD) (Hakimdavoodi and Amirmazlaghani, 2020). These findings are consistent with previous literature, showing impaired structural and functional connectivities within these networks in ADHD cohorts (Choi et al., 2013; McLeod et al., 2014; Bos et al., 2017). Due to its advantages over other dFC models and its good interpretability, it is advisable to use the AR-DCC model to enhance the detection of temporal dynamic characteristics of the thalamocortical FC in patients with MDD.

Most studies investigating thalamocortical FC in MDD have treated the thalamus as a uniform anatomical entity. This approach limits the ability to make precise inferences about specific locations of thalamocortical FC abnormalities. It is now recognized that the thalamus is a complex structure, composed of multiple nuclei with distinct projections to different areas of the cerebral cortex (Behrens et al., 2003). For example, the intralaminar and medial thalamic nuclei, which are primarily connected with frontoparietal and prefrontal areas, have been linked to various cognitive functions such as attention and reward-related behavior

(Saalmann, 2014). The anterior thalamic nuclei, connected with the frontal and limbic cortices, play a crucial role in memory processing and affective cognition (Dupire et al., 2013; Sweeney-Reed et al., 2021). The ventral thalamic nuclei have a projection to motor and premotor regions, and dysfunctions in these nuclei may affect attention biases toward positive stimuli in MDD (Gotlib et al., 2011; Hamilton et al., 2015). Recent investigations have sought to explore thalamocortical FC abnormalities in MDD by dividing the thalamus into different subregions. These studies have revealed subregion-dependent alterations in thalamocortical connectivity in patients with MDD (Kong et al., 2018; Xue et al., 2019). However, whether MDD is associated with aberrant dynamic functional interactions between thalamic subfields and cortical regions remains an open question.

In this study, we used the AR-DCC model and a precise thalamic atlas comprising ten subregions to analyze rs-fMRI data from 48 patients with MDD and 57 healthy controls (HCs). Our primary goal was to examine the presence of abnormal thalamocortical dFC patterns in patients with MDD, with a specific focus on temporal properties, dFC variability, and laterality dynamics, which could be associated with clinical symptoms. Specifically, we first used the *k*-means clustering method to identify distinct dFC states in the thalamocortical system. Four temporal properties and dFC variability were then computed to capture time-varying changes in thalamocortical FC patterns. In addition, we conducted dynamic laterality analysis to assess the changes in functional lateralization within the thalamocortical system over time.

2 Methods

2.1 Participants

A total of 123 participants, including 58 patients with MDD and 65 age- and sex-matched HCs, were recruited. MDD patients were enrolled from Gansu Provincial Hospital (Lanzhou, China) and diagnosed by the Structured Clinical Interview for the fourth version of Diagnostic and Statistical Manual of Mental Disorders (DSM-IV) Axis I Disorders (SCID). The HCs were enrolled through newspaper advertisements and were interviewed by the Structured Clinical Interview for DSM-IV (non-patient edition). The 17-item Hamilton Rating Scale for Depression (HAMD) (Hamilton, 1967) was used to assess the severity of depressive symptoms for each participant. All patients with MDD included in this study had a total score of ⩾8 on the HAMD (Williams, 1988; Long et al., 2020). The exclusion criteria in this work included: the presence of other major psychiatric diseases, a declared history of illegal substance abuse, the presence of severe physical illness, organic brain disease, left-handedness, and/or pregnancy. Then, the data from ten MDD patients and eight HCs were excluded from the study due to low image quality, evident head motion, and inadequate segmentation of thalamic nuclei (refer to Sections 2.3 and 2.4 for details). As a result, further analysis used the remaining dataset comprising 48 MDD patients and 57 HCs. Detailed demographic and clinical information is shown in Table 1.

2.2 Data acquisition

MRI data were acquired via a 3.0T Siemens Trio scanner (Siemens, Erlangen, Germany). The T1-weighted data were obtained with the following parameters: repetition time (t_R)/echo time (t_E)=2530 ms/3.39 ms, inversion time=1100 ms, matrix size=256×256, flip angle=7°, and sagittal slice number=128. The rs-fMRI data were collected using an echo-planar imaging sequence with the following parameters: t_R/t_E=2000 ms/30 ms, matrix size=64×64, flip angle=90°, field of view=220 mm×220 mm, slice number=33, slice thickness=3.5 mm, slice gap=0.6 mm, and a total of 240 volumes.

2.3 Data preprocessing

The T1-weighted data were preprocessed using FreeSurfer v7.2.0 (Fischl, 2012). Specifically, the "recon-all" function with default settings was performed, which included skull-stripping, motion correction, Talairach registration, intensity normalization, white matter labeling, topology correction and surface deformation, and segmentation of cortical and subcortical brain structures. Then, the Euler number, an automated quality control strategy provided by FreeSurfer, was used to exclude potential outliers (Rosen et al., 2018), i.e., patients with an Euler number below Q1−1.5×interquartile range or above Q3+1.5×interquartile range (only one MDD patient).

The rs-fMRI data were preprocessed using a MATLAB toolbox called Data Processing Assistant for

Resting-State fMRI (DPARSF) (Yan and Zang, 2010) based on the Statistical Parametric Mapping (SPM; https://www.fil.ion.ucl.ac.uk/spm). The preprocessing procedure was as follows: (1) removal of the first ten volumes; (2) slice timing and head motion correction; (3) nuisance covariate regression (including the white matter signal, cerebrospinal signal, linear trends, and Friston's 24 motion parameters); (4) spatial normalization to the Montreal Neurological Institute (MNI) space with 3 mm×3 mm×3 mm resolution; (5) spatial smoothing using an 8-mm full-width at half maximum Gaussian kernel; (6) band-pass filtering at 0.01–0.08 Hz. Participants with a head displacement of >2 mm, rotation angle of >2°, or mean frame-wise displacement (FD) of >0.2 mm were excluded to minimize the effect of head motion (including seven MDD patients and four HCs).

2.4 Definition of thalamic subregions

The ThalamicNuclei pipeline in FreeSurfer v7.2.0 (Fischl, 2012) was used to segment thalamic nuclei. Briefly, the probabilistic thalamic segmentation algorithm was performed on the preprocessed T1-weighted images to segment the whole thalamus into 50 different subregions (Iglesias et al., 2018). The automatic segmentation of each participant was then visually inspected to assess the segmentation quality of thalamic nuclei. As a result, data from two MDD patients and four HCs with biologically implausible segmentation of nuclei groups were discarded. Next, we grouped thalamic nuclei into five different subregions for each side in the native space according to previous studies (Weeland et al., 2022a, 2022b), including anterior, lateral, ventral, intralaminar/medial, and pulvinar subregions (Table S1, Fig. 1a). The thalamic mask of each participant was spatially normalized to the MNI space using the Advanced Normalization Tools (ANTs) (Avants et al., 2009).

2.5 Auto-regressive dynamic conditional correlation model for dynamic functional connectivity analysis

The cortex was divided into 200 regions of interest (ROIs) according to the Schaefer atlas (Schaefer et al., 2018) (Fig. 1a). For each participant, the mean time courses of 10 thalamic subregions and 200 cortical regions were extracted. Then, the AR-DCC model that combines the AR and DCC models was applied to estimate the dFC patterns between 10 thalamic subregions and 200 cortical regions (Hakimdavoodi and Amirmazlaghani, 2020). Compared with the sliding-window method, the AR-DCC model eliminates the need for window size adjustments, enabling the estimation of the FC between each pair of brain regions at each time point. Assume that $\boldsymbol{Y}_t$ (t=1, 2, ..., T) is an N-dimensional time series:

$$\boldsymbol{Y}_t = \boldsymbol{M}_t + \boldsymbol{X}_t, \boldsymbol{Y}_t := \left[y_{1,t}, y_{2,t}, ..., y_{N,t} \right]^{\mathrm{T}}, \quad (1)$$

where t is a time in the time series in each region, N is the number of brain regions, $\boldsymbol{M}_t$ is computed via the N different AR models, and $\boldsymbol{X}_t$ is estimated using the DCC model.

The first part of the AR-DCC model estimates the temporal autocorrelation of the fMRI time series through an AR model, such as low-frequency correlations caused by equipment and wide-band correlations caused by underlying physiological fluctuations (Purdon and Weisskoff, 1998; Lund et al., 2006). Specifically, N-dimensional time series $\boldsymbol{Y}_t$ (t=1, 2, ..., T) follows the N different AR models of order p, which can be written as follows:

$$y_{d,t} = a_{d,0} + \sum_{k=1}^{p} a_{d,k} y_{d,t-k} + x_{d,t},\ x_{d,t} \sim N\left(0, \delta_d^2\right),$$
$$d = 1, 2, ..., N, \quad (2)$$

where $y_{d,t}$ is the dth element of $\boldsymbol{Y}_t$, $a_{d,0}$, $a_{d,k} \neq 0$ (k=1, 2, ..., p) are AR parameters, and $x_{d,t}$ is the dth element of $\boldsymbol{X}_t$ with a zero mean and a variance δ_d^2.

The second part of the AR-DCC model considers the correlation changes estimated by the DCC model fitted on the AR residuals. Assuming that $\boldsymbol{X}_t$ is an N-dimensional mean zero time series, the dynamic correlation matrix $\boldsymbol{R}_t$ can be calculated as follows:

$$h_{i,t} = \omega_i + \alpha_i \boldsymbol{X}_{i,t-1}^2 + \beta_i h_{i,t-1}, i = 1, 2, ..., N, \quad (3)$$

$$\boldsymbol{D}_t = \mathrm{diag}\left(h_{1,t}^{1/2}, h_{2,t}^{1/2}, ..., h_{N,t}^{1/2} \right), \quad (4)$$

$$\boldsymbol{U}_t = [\, u_{1,t}, u_{2,t}, ..., u_{N,t} \,]^{\mathrm{T}} \text{ with } u_{i,t} = \boldsymbol{D}_{i,t}^{-1} \boldsymbol{X}_{i,t},$$
$$i = 1, 2, ..., N, \quad (5)$$

$$\boldsymbol{Q}_t = \left(1 - \gamma - \kappa\right) E\left[\boldsymbol{U}_t \boldsymbol{U}_t^{\mathrm{T}}\right] + \gamma\left(\boldsymbol{U}_{t-1} \boldsymbol{U}_{t-1}^{\mathrm{T}}\right) + \kappa \boldsymbol{Q}_{t-1}, \quad (6)$$

$$\boldsymbol{R}_t = \mathrm{diag}\left(\boldsymbol{Q}_t\right)^{-\frac{1}{2}} \boldsymbol{Q}_t \mathrm{diag}\left(\boldsymbol{Q}_t\right)^{-\frac{1}{2}}. \quad (7)$$

The second part of the AR-DCC model can be split into the following steps. Firstly, fitting the generalized autoregressive conditional heteroscedastic (GARCH) model to each time series within $\boldsymbol{X}_t$, the

conditional standard deviation $h_{i,t}$ of the ith time-series is modeled as a linear combination of $h_{i,t-1}$ and $\boldsymbol{X}^2_{i,t-1}$ (Eq. (3)). Secondly, the standardized residual $\boldsymbol{U}_t$ is computed through Eqs. (4) and (5). The $\boldsymbol{D}_t$ in Eq. (4) is a diagonal matrix, and the ith diagonal element corresponds to $h_{i,t}$. Thirdly, an exponentially weighted moving average (EWMA) window is applied to the $\boldsymbol{U}_t$ to compute a non-normalized version of the time-varying correlation matrix termed as $\boldsymbol{Q}_t$ (Eq. (6)). The $E\left[\boldsymbol{U}_t\boldsymbol{U}_t^{\mathrm{T}}\right]$ in Eq. (6) represents the unconditional covariance matrix of $\boldsymbol{U}_t$. Finally, $\boldsymbol{Q}_t$ is rescaled to ensure a proper correlation matrix $\boldsymbol{R}_t$ being created (Eq. (7)). The $\mathrm{diag}(\boldsymbol{Q}_t)$ in Eq. (7) is a diagonal matrix formed by diagonal elements of $\boldsymbol{Q}_t$. The ω_i, α_i, β_i, γ, and κ are non-negative parameters of the DCC model, estimated by the quasi-maximum likelihood method.

As a result, a total of 230-time windows were obtained for each participant and a 10×200 thalamocortical correlation matrix was computed for each window. To assess recurring dFC patterns over time, the k-means clustering method was performed on all correlation matrices of all participants (Allen et al., 2014). The L1 distance was used as a similarity measure between matrices (Aggarwal et al., 2001) and the k-means clustering method was iterated 200 times with random initialization of cluster centroids to escape local minima (Allen et al., 2014). Here, the optimal solution of clusters was determined by the elbow criterion with k varying from 2 to 10 (Calhoun et al., 2014). After clustering, each participant obtained a state vector representing changes in dFC states over time. Finally, four measures were calculated to estimate temporal properties of dFC states, including (1) fractional time, defined as the proportion of time spent in each state; (2) mean dwell time, defined as the average number of consecutive windows in a certain state before switching to another state; (3) number of transitions between different states; (4) transition probability, defined as the probability of switching from one state to another state. Moreover, we also calculated the variance of FC across all windows clustered into one state, i.e., dFC variability, to characterize the thalamocortical dFC fluctuations. The pipeline of dFC analysis is shown in Fig. 1.

2.6 Dynamic laterality analysis

To capture the dynamics of laterality in the thalamocortical circuit, we calculated a dynamic laterality index (DLI) for each thalamic subregion at each time window (Chen et al., 2019; Wu et al., 2022). The DLI at the tth window is defined as

$$\mathrm{DLI}_t = \frac{\sum_{j=1}^{n} r(\mathrm{ROI}_i, \mathrm{ROI}_j)}{n} - \frac{\sum_{k=1}^{m} r(\mathrm{ROI}_i, \mathrm{ROI}_k)}{m}, \tag{8}$$

where $\frac{1}{n}\sum_{j=1}^{n} r(\mathrm{ROI}_i, \mathrm{ROI}_j)$ indicates the averaged FC strength between the ith thalamic ROI and all cortical regions in the left hemisphere; $\frac{1}{m}\sum_{k=1}^{m} r(\mathrm{ROI}_i, \mathrm{ROI}_k)$ indicates the averaged FC strength between the ith thalamic ROI and all cortical regions in the right hemisphere. j represents jth cortical region in the left hemispheres; k represents kth cortical region in the right hemispheres; n and m represent the numbers of cortical regions in the left and right hemispheres, respectively. Then, a measure termed laterality fluctuation (LF), defined as the variance of the time series of DLI across all windows, was computed to characterize the dynamic changes in laterality during the whole scan.

2.7 Dynamic functional connectivity analysis of thalamo-subnetwork connectivity

Previous analyses conducted on the thalamus and the entire cortex only emphasized the global dynamic interactions of the thalamocortical system, potentially neglecting important insights into abnormal dFC patterns within local thalamocortical circuits (i.e., dynamic interactions between the thalamus and functional subnetworks). In this study, the 200 cortical regions were categorized into seven networks, including the visual network (Vis), somatomotor network (SomMot), dorsal attention network (DorsAttn), salient ventral attention network (SalVentAttn), limbic network (Limbic), executive control network (Cont), and default mode network (Default). We then investigated local dFC patterns of the thalamocortical system using the experimental procedure mentioned in Sections 2.5 and 2.6.

2.8 Statistical analysis

Group differences in age and sex were examined using the two-sample t-test and Chi-square test, respectively. A non-parametric permutation test (5000 repetitions), with age and sex as covariates, was performed to investigate the statistical significance of

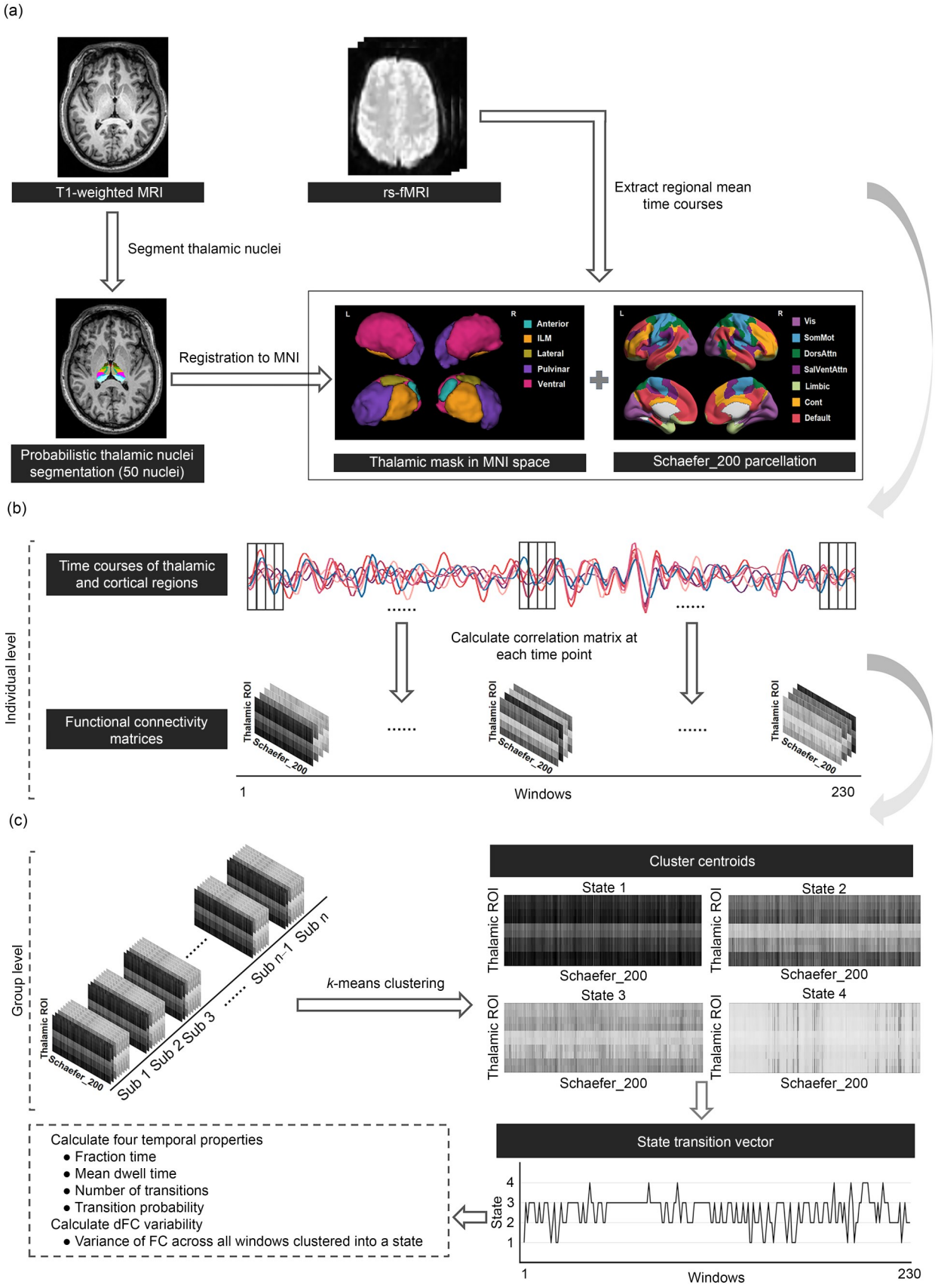
(a)
T1-weighted MRI
rs-fMRI
Extract regional mean time courses
Segment thalamic nuclei
Registration to MNI
Probabilistic thalamic nuclei segmentation (50 nuclei)
Anterior
iLM
Lateral
Pulvinar
Ventral
Thalamic mask in MNI space
Vis
SomMot
DorsAttn
SalVentAttn
Limbic
Cont
Default
Schaefer_200 parcellation
(b)
Individual level
Time courses of thalamic and cortical regions
Calculate correlation matrix at each time point
Functional connectivity matrices
Thalamic ROI
Schaefer_200
1
Windows
230
(c)
Group level
Sub 1
Sub 2
Sub 3
Sub n-1
Sub n
k-means clustering
Cluster centroids
State 1
State 2
State 3
State 4
Calculate four temporal properties
• Fraction time
• Mean dwell time
• Number of transitions
• Transition probability
Calculate dFC variability
• Variance of FC across all windows clustered into a state
State transition vector
State
4
3
2
1

Fig. 1 Pipeline of dynamic functional connectivity (dFC) analysis in thalamocortical connectivity. (a) Identification of thalamic and cortical regions. The thalamus was segmented into 50 thalamic nuclei using a probabilistic thalamic segmentation algorithm in FreeSurfer. Then, the 50 nuclei were grouped into five thalamic subregions for each side (including anterior thalamus (Anterior), lateral thalamus (Lateral), ventral thalamus (Ventral), intralaminar/medial thalamus (ILM), and pulvinar thalamus (Pulvinar)), and spatially normalized to the Montreal Neurological Institute (MNI) space. The 200 cortical regions were defined by the Schaefer atlas, which was categorized into seven networks including visual network (Vis), somatomotor network (SomMot), dorsal attention network (DorsAttn), salient ventral attention network (SalVentAttn), limbic network (Limbic), executive control network (Cont), and default mode network (Default). The regional mean time courses of ten thalamic regions and 200 cortical regions were extracted. (b) Estimation of thalamocortical dFC patterns. The auto-regressive dynamic conditional correlation (AR-DCC) model was used to obtain 230 correlation matrices (10×200) for each participant. (c) Thalamocortical dFC state analysis. Correlation matrices of all participants were clustered into four dFC states using the *k*-means clustering algorithm. Four temporal properties (i.e., fractional time, mean dwell time, number of transitions, and transition probability) and the dFC variability were calculated for analysis. MRI: magnetic resonance imaging; rs-fMRI: resting-state functional MRI; ROI: region of interest.

changes in the dFC metrics (i.e., four temporal properties, dFC variability, and LF) in MDD patients relative to the HCs. Briefly, we first calculated the real between-group difference of each metric. To determine whether the group differences could occur by chance, we then randomly reassigned all participants into the two groups and recomputed the differences between the two randomized groups based on each metric. This randomization procedure was repeated 5000 times, which could result in a null distribution of between-group differences. An observed difference value outside the 95% confidence interval of the distribution indicated the existence of statistical difference for a given metric between the two groups. Multiple comparisons were corrected via the false discovery rate (FDR) method at the level of q=0.05. The Pearson correlation coefficients between altered dFC metrics (i.e., four temporal properties, dFC variability, and LF) and clinical data (i.e., HAMD, the Hamilton Rating Scale for Anxiety (HAMA), and illness duration) were calculated for the MDD group.

3 Results

3.1 Demographic characteristics

A total of 48 MDD patients and 57 HCs were included in the current study. As shown in Table 1, no significant differences were detected between MDD and HC groups in age (P=0.989), sex (P=0.561), or mean FD (P=0.291).

3.2 Dynamic functional connectivity between the thalamus and the whole cortex

3.2.1 Dynamics of thalamocortical connectivity

Four recurring states of thalamocortical connectivity were identified using *k*-means clustering (Figs. 2a and S1a). State 1 (15.5%) and state 4 (9.2%) were less frequent than state 2 (30.1%) and state 3 (45.2%). State 1 showed highly positive correlations between the thalamus and the whole cerebral cortex. The connectivity patterns of state 2 and state 3 resembled those of state 1, but were accompanied by a reduced connectivity strength. State 4 showed strong negative connectivity between the thalamus and primary cortical networks (e.g., Vis and SomMot) and less positive thalamic connectivity with higher-order cortical networks (e.g., DorsAttn, SalVentAttn, Cont, and Default). Compared with the HCs, patients with MDD exhibited significantly decreased fractional time in state 4 and reduced transition probability from both state 2 and state 3 to state 4 (all P<0.05, with FDR corrected; Figs. 2b and S1b). No significant between-group differences were found in dFC variability.

Table 1 Demographic and clinical characteristics of participants

Group	Age (years)	Sex (female/male)	HAMA	HAMD (17-item)	Illness duration (years)	Mean FD (mm)
MDD (n=48)	33.67±12.45	24/24	17.92±6.66	18.56±6.18	4.50 (1.52, 8.18)	0.07±0.04
HCs (n=57)	33.70±12.41	32/25				0.08±0.04
P	0.989[a]	0.561[b]				0.291[a]

Data are displayed as mean±standard deviation (SD), except numbers for sex or illness duration which is presented as median (interquartile range (IQR)). MDD: major depressive disorder; HCs: healthy controls; HAMA: Hamilton Rating Scale for Anxiety; HAMD: Hamilton Rating Scale for Depression; FD: frame-wise displacement. [a] P values for the two-sample t-test; [b] P values for the Chi-square test.

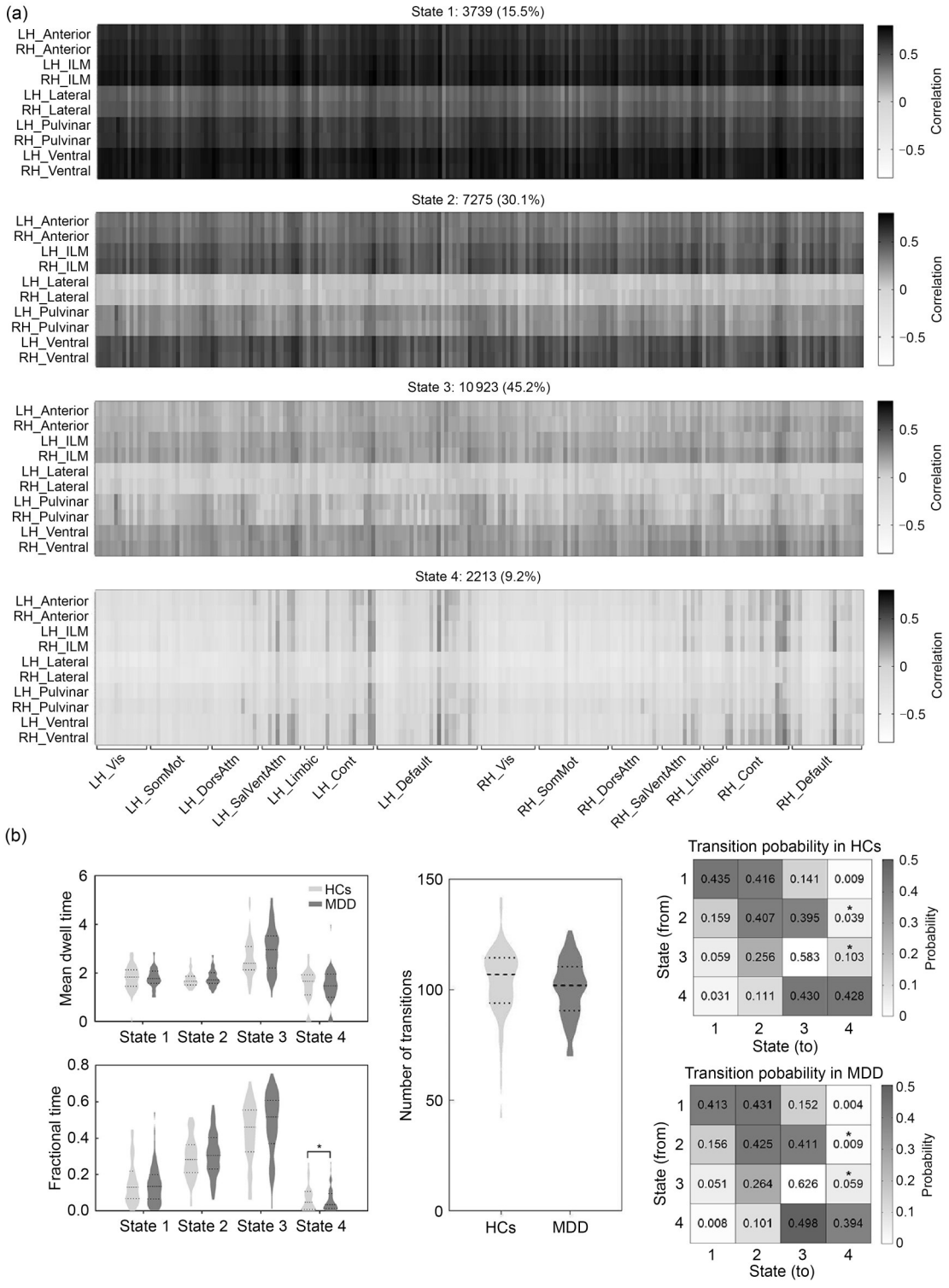

Fig. 2 Temporal properties of thalamocortical connectivity. (a) Cluster centroids for each state in thalamocortical connectivity. The total number and percentage of state occurrences are listed above each centroid. (b) Temporal properties of thalamocortical dynamic functional connectivity (dFC) states. * P_{FDR}<0.05. FDR: false discovery rate; LH: left hemisphere; RH: right hemisphere; Anterior: anterior thalamus; ILM: intralaminar/medial thalamus; Lateral: lateral thalamus; Pulvinar: pulvinar thalamus; Ventral: ventral thalamus; Vis: visual network; SomMot: somatomotor network; DorsAttn: dorsal attention network; SalVentAttn: salient ventral attention network; Limbic: limbic network; Cont: executive control network; Default: default mode network; HCs: healthy controls; MDD: major depressive disorder.

To assess the influence of smoothing kernel size on our data, we compared the effect of the 6-mm and 8-mm smoothing kernels on both the thalamus and thalamocortical circuit scales. The thalamic activation and thalamocortical FC patterns at 6 mm were remarkably similar to those at 8 mm (Fig. S2, Table S2), suggesting that the size of smoothing kernels did not significantly influence the results of the analysis.

In addition, we also re-performed the dFC analysis on the global thalamocortical circuits via the sliding window method with a window size of 50 TR and a step of 1 TR. After the *k*-means clustering analysis, we also obtained four thalamocortical dFC states, whose patterns were largely consistent with the results of the AR-DCC model (Fig. S3). However, no significant between-group differences were found in the four temporal properties (Table S3). In contrast, the AR-DCC model is more sensitive in capturing dFC patterns that MDD patients showed significantly decreased fractional time and reduced transition probability between dFC states.

3.2.2 Dynamic laterality index analysis

The functional laterality of the thalamocortical system in MDD altered considerably over all time windows. As shown in Fig. 3a, the LFs of the bilateral anterior thalamus, intralaminar/medial thalamus, pulvinar thalamus, and ventral thalamus significantly increased in patients with MDD relative to the HCs (all $P<0.05$, with FDR corrected).

3.3 Dynamic functional connectivity between the thalamus and cortical subnetworks

3.3.1 Dynamics of thalamo-subnetwork connectivity

We identified five recurring dFC states in the thalamo-Vis (Figs. 4a and S4a), thalamo-SomMot (Figs. 5a and S5a), thalamo-Limbic (Fig. S6a), thalamo-Default (Fig. S7), and thalamo-DorsAttn (Fig. S8a) connectivity, and four states in the thalamo-Cont (Fig. S6b) and thalamo-SalVentAttn (Fig. S8b) connectivity. The detailed characteristics of all states are summarized in Table 2. Compared to the analysis between the thalamus and the whole cortex, the thalamo-subnetwork analysis offered a deeper understanding of the dynamic pattern of interaction between the thalamus and each subnetwork. The more dFC states we identified within these local circuits indicated that thalamo-subnetwork analysis could provide a more comprehensive understanding of the dynamic changes in local loops. Such changes could not be completely

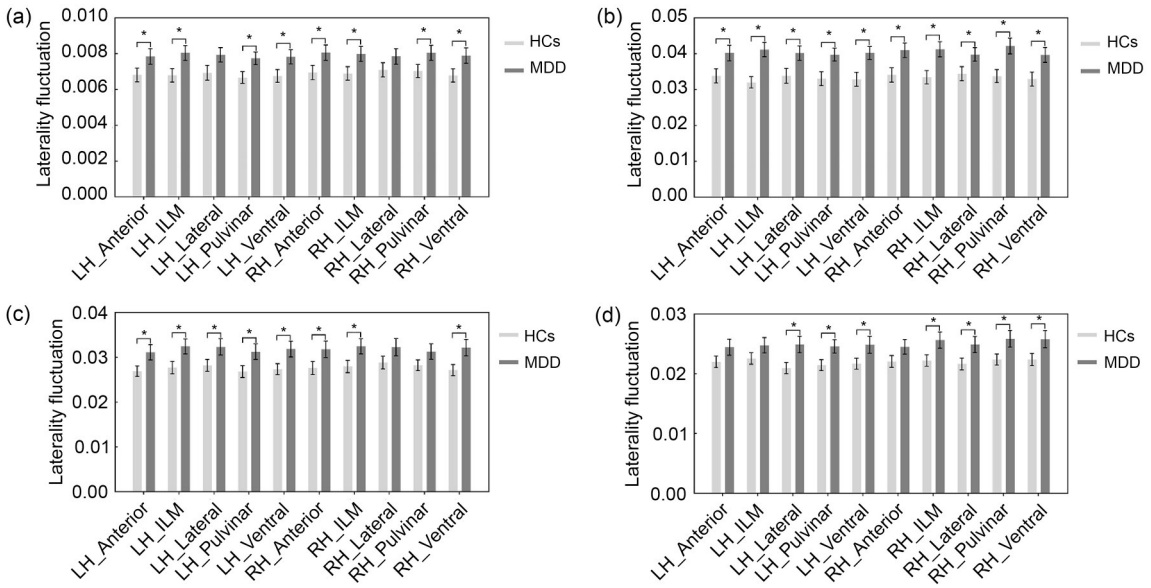

Fig. 3 Results of dynamic laterality analysis. (a) The laterality fluctuations (LFs) in thalamic connectivity with the whole cortex. (b–d) LF in thalamic connectivity with the Cont (b), DorsAttn (c), and SalVentAttn (d) networks. * $P_{FDR}<0.05$. Data are displayed as mean±standard error of the mean (SEM), *n*=48 (MDD) or *n*=57 (HCs). FDR: false discovery rate; LH: left hemisphere; RH: right hemisphere; Anterior: anterior thalamus; ILM: intralaminar/medial thalamus; Lateral: lateral thalamus; Pulvinar: pulvinar thalamus; Ventral: ventral thalamus; Cont: executive control network; DorsAttn: dorsal attention network; SalVentAttn: salient ventral attention network; HCs: healthy controls; MDD: major depressive disorder.

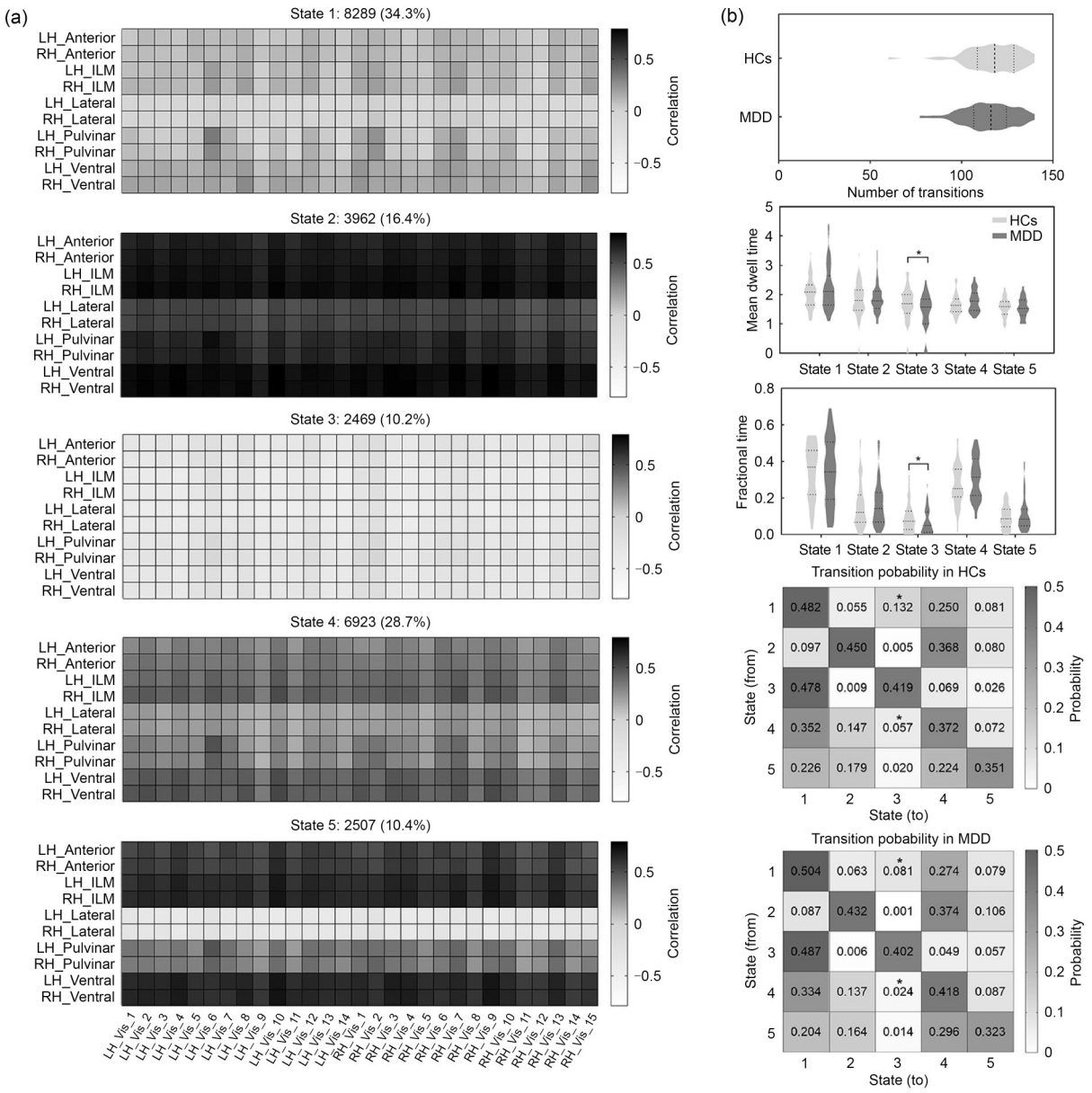

Fig. 4 Temporal properties of thalamo-Vis connectivity. (a) Cluster centroids for each state in thalamo-Vis connectivity. The total number and percentage of state occurrences are listed above each centroid. (b) Temporal properties of dynamic functional connectivity (dFC) states in thalamo-Vis connectivity. * P_{FDR}<0.05. FDR: false discovery rate; LH: left hemisphere; RH: right hemisphere; Anterior: anterior thalamus; ILM: intralaminar/medial thalamus; Lateral: lateral thalamus; Pulvinar: pulvinar thalamus; Ventral: ventral thalamus; Vis: visual network; Vis_[*i*]: the *i*th region of the visual network; HCs: healthy controls; MDD: major depressive disorder.

captured when considering the thalamocortical circuit as a whole.

Regarding the temporal properties, significant group differences in the thalamocortical system were observed only between the thalamus and primary cortical networks (e.g., Vis and SomMot) (all P<0.05, with FDR corrected). Specifically, for the thalamo-Vis system, MDD patients showed decreased fractional time and mean dwell time in state 3, as well as a lower probability of transition from both state 1 and state 4 to state 3 relative to the HCs (Figs. 4b and S4b). Moreover, a significant decrease in fractional time of state 2 in the thalamo-SomMot system was also observed in MDD patients (Figs. 5b and S5b).

The comparison of the dFC variability between the two groups showed significant differences in

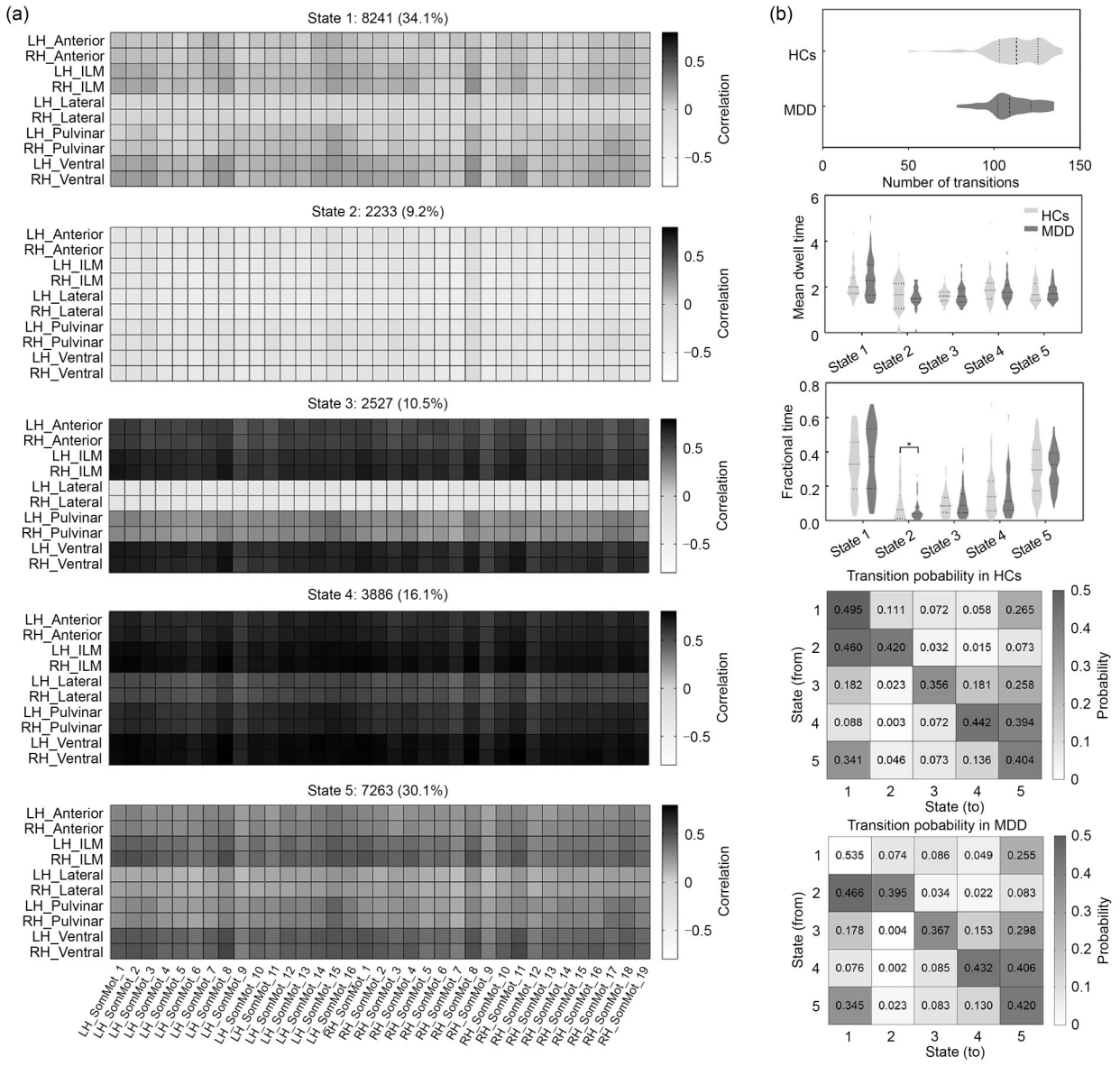

Fig. 5 Temporal properties of thalamo-SomMot connectivity. (a) Cluster centroids for each state in thalamo-SomMot connectivity. The total number and percentage of state occurrences are listed above each centroid. (b) Temporal properties of dynamic functional connectivity (dFC) states in thalamo-SomMot connectivity. * P_{FDR}<0.05. FDR: false discovery rate; LH: left hemisphere; RH: right hemisphere; Anterior: anterior thalamus; ILM: intralaminar/medial thalamus; Lateral: lateral thalamus; Pulvinar: pulvinar thalamus; Ventral: ventral thalamus; SomMot: somatomotor network; SomMot_[*i*]: the *i*th region of the somatomotor network; HCs: healthy controls; MDD: major depressive disorder.

connectivity between the thalamus and higher-order cortical networks (e.g., Default, DorsAttn, and SalVentAttn) (all P<0.05, with FDR corrected). In state 5, the MDD patients showed significant differences in the thalamo-Default connectivity (Fig. 6a). Specifically, a significant increase in dFC variability was observed between the left middle temporal gyrus and the right intralaminar/medial thalamus, as well as the left anterior, pulvinar, and ventral thalami. There was also significantly more dFC variability between the right medial superior frontal gyrus and the left pulvinar thalamus and between the right superior frontal gyrus and all the bilateral anterior, intralaminar/medial, and ventral thalami. The thalamo-DorsAttn circuit in state 5 also showed significant increases in dFC variability for connectivity linking the right superior frontal gyrus with the left

Table 2 Summary of the thalamo-subnetwork connectivity characteristics of all states

Thalamo-subnetwork connectivity	State	Frequency of different states (%)	Connectivity pattern
Thalamo-Vis	1	34.3	Weak positive connectivity state
	2	16.4	Strong positive connectivity state
	3	10.2	Strong negative connectivity state
	4	28.7	Moderate positive connectivity state
	5	10.4	Strong positive connectivity state, but has negative connections with bilateral lateral thalamic nuclei
Thalamo-SomMot	1	34.1	Weak positive connectivity state
	2	9.2	Strong negative connectivity state
	3	10.5	Strong positive connectivity state, but has negative connections with bilateral lateral thalamic nuclei
	4	16.1	Strong positive connectivity state
	5	30.1	Moderate positive connectivity state
Thalamo-Default	1	27.2	Moderate positive connectivity state
	2	9.9	Strong positive connectivity state, but has negative connections with bilateral lateral thalamic nuclei
	3	11.4	Strong negative connectivity state
	4	36.6	Weak positive connectivity state
	5	14.9	Strong positive connectivity state
Thalamo-DorsAttn	1	36.7	Weak positive connectivity state
	2	10.6	Strong negative connectivity state
	3	10.6	Strong positive connectivity state, but has negative connections with bilateral lateral thalamic nuclei
	4	15.1	Strong positive connectivity state
	5	27.0	Moderate positive connectivity state
Thalamo-Limbic	1	11.4	Strong positive connectivity state, but has negative connections with the bilateral orbital frontal cortex
	2	23.9	Moderate positive connectivity state
	3	15.1	Strong positive connectivity state
	4	36.9	Weak positive connectivity state
	5	12.7	Strong negative connectivity state
Thalamo-SalVentAttn	1	28.8	Moderate positive connectivity state
	2	41.1	Weak positive connectivity state
	3	16.9	Strong positive connectivity state
	4	13.2	Strong negative connectivity state
Thalamo-Cont	1	28.0	Moderate positive connectivity state
	2	15.7	Strong negative connectivity state, but has positive connections with bilateral cingulate and right prefrontal cortex
	3	16.0	Strong positive connectivity state
	4	40.3	Weak positive connectivity state

Vis: visual network; SomMot: somatomotor network; Default: default mode network; DorsAttn: dorsal attention network; Limbic: limbic network; SalVentAttn: salient ventral attention network; Cont: executive control network.

intralaminar/medial thalamus, right lateral thalamus, and bilateral ventral thalamus in MDD patients (Fig. 6b). For the thalamo-SalVentAttn connectivity, MDD patients showed increased dFC variability

between the right intralaminar/medial thalamus and left insula in state 1 (Fig. 6c). No significant between-group difference was observed in temporal properties or dFC variability for the thalamo-Cont and thalamo-Limbic circuits.

3.3.2 Dynamic laterality index analysis of thalamo-subnetwork connectivity

Compared to the HCs, MDD patients showed greater variation across the scan duration in functional laterality of connectivity between the thalamus and higher-order cortical networks (e.g., Cont, DorsAttn, and SalVentAttn) (all $P<0.05$, with FDR corrected; Figs. 3b–3d). Specifically, significantly increased LF was found in the bilateral ventral thalamus (involving the thalamo-Cont, thalamo-DorsAttn, and thalamo-SalVentAttn circuits), bilateral anterior thalamus and intralaminar/medial thalamus (involving the thalamo-Cont and thalamo-DorsAttn circuits), bilateral lateral thalamus and pulvinar thalamus (involving the

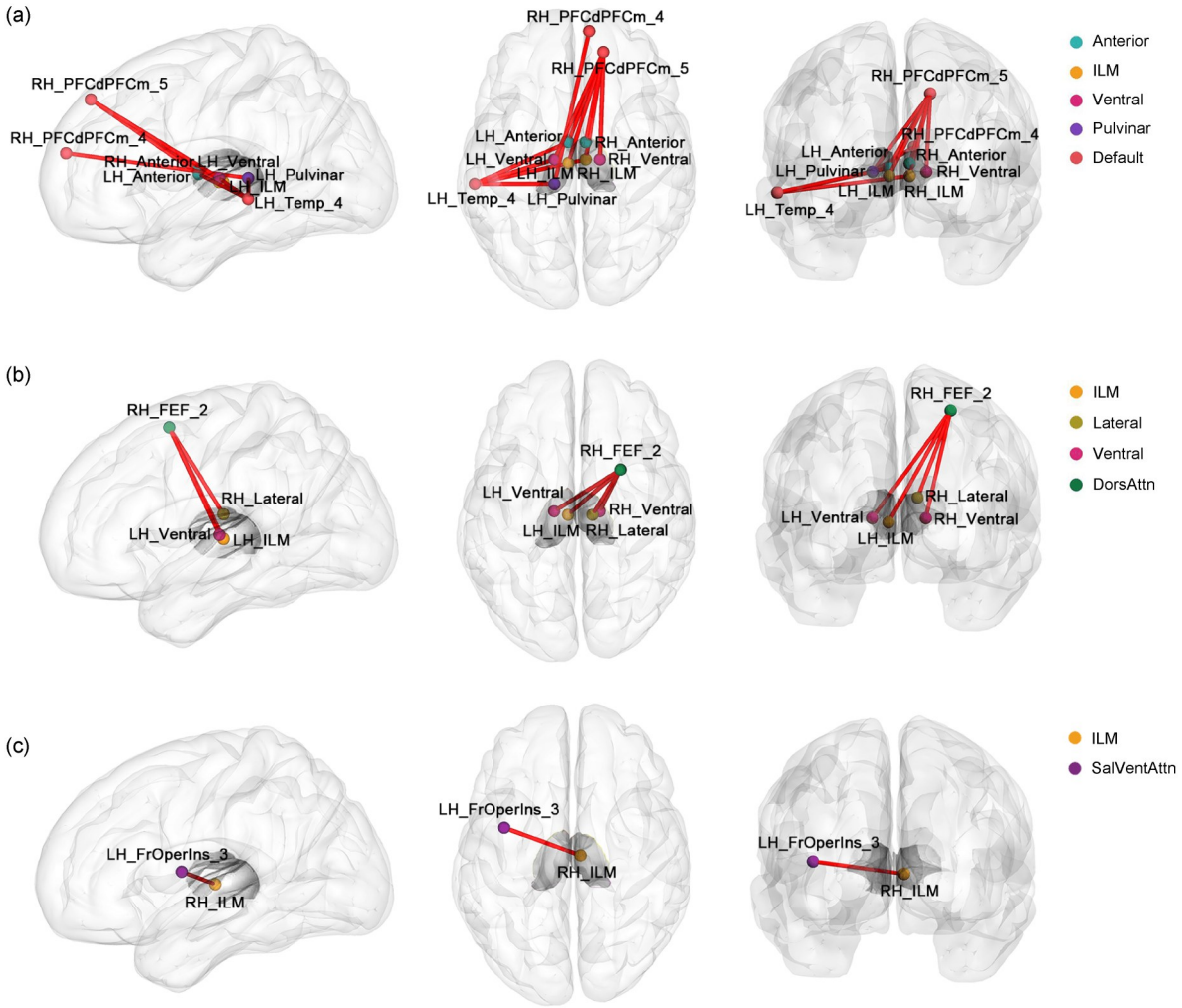

Fig. 6 Thalamo-subnetwork connectivity with significant variability changes in major depressive disorder (MDD) patients. Dynamic functional connectivity (dFC) variability was altered in the thalamo-Default (in state 5) (a), thalamo-DorsAttn (in state 5) (b), and thalamo-SalVentAttn (in state 1) (c) circuits. The red lines indicate a significant increase in dFC variability in MDD patients compared to the HCs. LH: left hemisphere; RH: right hemisphere; Anterior: anterior thalamus; ILM: intralaminar/medial thalamus; Lateral: lateral thalamus; Pulvinar: pulvinar thalamus; Ventral: ventral thalamus; Default: default mode network; DorsAttn: dorsal attention network; SalVentAttn: salient ventral attention network; Temp_4: the fourth region of the temporal cortex (middle temporal gyrus); PFCdPFCm_4: the fourth region of the dorsal/medial prefrontal cortex (medial superior frontal gyrus); PFCdPFCm_5: the fifth region of the dorsal/medial prefrontal cortex (superior frontal gyrus); FEF_2: the second region of the frontal eye fields (superior frontal gyrus); FrOperIns_3: the third region of the frontal operculum insula (insula).

thalamo-Cont and thalamo-SalVentAttn circuits), left lateral thalamus and pulvinar thalamus (involving the thalamo-DorsAttn circuit), and right intralaminar/medial thalamus (involving the SalVentAttn circuit).

3.4 Correlations with clinical characteristics

The HAMD score was negatively correlated with the dFC variability between the left anterior thalamus and left middle temporal gyrus in state 5 in the thalamo-Default connectivity (r=−0.296, P=0.041 (uncorrected); Fig. 7a), and positively correlated with the dFC variability between the right lateral thalamus and right superior frontal gyrus in state 5 in the thalamo-DorsAttn connectivity (r=0.339, P=0.018 (uncorrected); Fig. 7b). These results suggest a clinically relevant association between the severity of MDD symptoms and abnormal dynamic functional interactions in the thalamocortical system. Other dynamic measures (including the LF and temporal properties) did not show a significant correlation with the clinical data.

4 Discussion

In this study, we investigated the changes in thalamocortical dFC patterns in patients with MDD from both whole-cortex and subnetwork perspectives. The major findings were as follows (Table 3): (1) MDD patients showed abnormal temporal properties in a negative connectivity state that was primarily involved in thalamic connectivity with primary cortical networks (e.g., Vis and SomMot); (2) the thalamo-subnetwork analysis detected more MDD-related nuances related to higher-order cortical networks (i.e., increased dFC variability between the thalamus and the Default, DorsAttn, and SalVentAttn), which had not been detected by the analysis at the thalamus-whole cortex level; (3) the functional lateralization of the thalamocortical system showed greater fluctuations over time in MDD patients, involving thalamo-Cont, thalamo-DorsAttn, and thalamo-SalVentAttn circuits; and (4) the dFC variability of thalamo-Default and thalamo-DorsAttn connectivity could predict the HAMD scores of patients with MDD. These findings suggest a heterogeneous pattern of changes in the impaired dynamics of thalamic interactions with both primary and higher-order cortical networks, which may be responsible for sensory and cognitive impairments in MDD. To our knowledge, this is the first comprehensive study of dFC alteration patterns within the thalamocortical circuitry in MDD patients. The results supplement current knowledge about the dysfunction of the thalamocortical system in depression.

The analysis of dFC between the thalamus and the whole cortex revealed that MDD patients showed decreased fractional time in the negative connectivity state (state 4) and fewer transitions from the positive connectivity states (states 2 and 3) to state 4. Previous studies have documented that positive connectivity can be taken as the synchronization and integration of brain neuronal activity, while negative connectivity refers to the segregation of brain neuronal activity with competitive representations (Fox et al., 2005, 2009). Thus, state 4 dominated by negative connectivity might represent a status of high segregation, while states 2 and 3 might represent highly integrated brain regions.

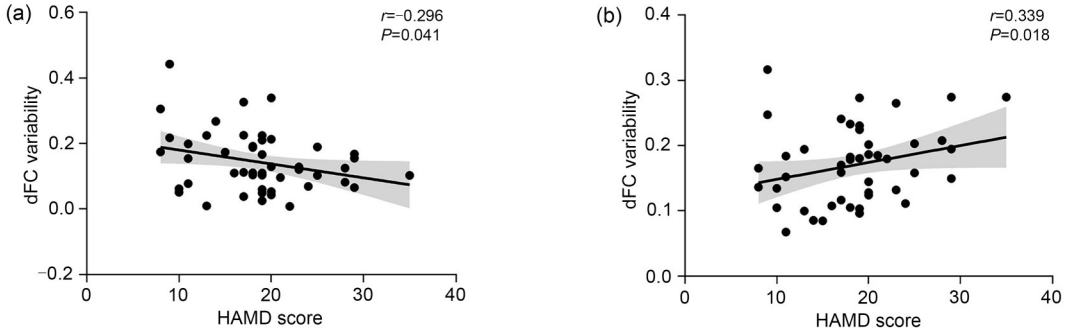

Fig. 7 Correlations between altered dFC variability and the HAMD score in MDD patients. (a) dFC variability between LH_Anterior and LH_Temp_4 in state 5 in thalamo-Default connectivity. (b) dFC variability between RH_Lateral and RH_FEF_2 in state 5 in thalamo-DorsAttn connectivity. dFC: dynamic functional connectivity; HAMD: Hamilton Rating Scale for Depression; LH: left hemisphere; RH: right hemisphere; Anterior: anterior thalamus; Lateral: lateral thalamus; Temp_4: the fourth region of the temporal cortex (middle temporal gyrus); FEF_2: the second region of the frontal eye fields (superior frontal gyrus).

Table 3 Summary of all statistical analysis results

Circuitry	Fractional time	Mean dwell time	Transition probability	dFC variability between the thalamus and cortex	LF in thalamus
Thalamo-cortical	State 4 ↓	ns	State 2 to state 4 ↓; State 3 to state 4 ↓	ns	Bilateral anterior, ILM, pulvinar, and ventral nuclei ↑
Thalamo-Vis	State 3 ↓	State 3 ↓	State 1 to state 3 ↓; State 4 to state 3 ↓	ns	ns
Thalamo-SomMot	State 2 ↓	ns	ns	ns	ns
Thalamo-Default	ns	ns	ns	LH_Anterior-LH_Temp_4 ↑ (*); RH_ILM-LH_Temp_4 ↑; LH_Ventral-LH_Temp_4 ↑; LH_Pulvinar-LH_Temp_4 ↑; LH_Pulvinar-RH_PFCdPFCm_4 ↑; LH_Anterior-RH_PFCdPFCm_5 ↑; RH_Anterior-RH_PFCdPFCm_5 ↑; LH_ILM-RH_PFCdPFCm_5 ↑; RH_ILM-RH_PFCdPFCm_5 ↑; LH_Ventral-RH_PFCdPFCm_5 ↑; RH_Ventral-RH_PFCdPFCm_5 ↑	ns
Thalamo-DorsAttn	ns	ns	ns	RH_Lateral-RH_FEF_2 ↑ (*); LH_ILM-RH_FEF_2 ↑; LH_Ventral-RH_FEF_2 ↑; RH_Ventral-RH_FEF_2 ↑	Bilateral anterior, ILM, ventral nuclei, and left lateral and pulvinar nuclei ↑
Thalamo-SalVentAttn	ns	ns	ns	RH_ILM-LH_FrOperIns_3 ↑	Bilateral lateral, pulvinar, ventral nuclei, and right ILM ↑
Thalamo-Cont	ns	ns	ns	ns	Bilateral anterior, ILM, lateral, pulvinar, and ventral nuclei ↑
Thalamo-Limbic	ns	ns	ns	ns	ns

LF: laterality fluctuation; LH: left hemisphere; RH: right hemisphere; Anterior: anterior thalamus; ILM: intralaminar/medial thalamus; Lateral: lateral thalamus; Pulvinar: pulvinar thalamus; Ventral: ventral thalamus; Vis: visual network; SomMot: somatomotor network; DorsAttn: dorsal attention network; SalVentAttn: salient ventral attention network; Limbic: limbic network; Cont: executive control network; Default: default mode network; Temp_4: the fourth region of the temporal cortex (middle temporal gyrus); PFCdPFCm_4: the fourth region of the dorsal/medial prefrontal cortex (medial superior frontal gyrus); PFCdPFCm_5: the fifth region of the dorsal/medial prefrontal cortex (superior frontal gyrus); FEF_2: the second region of the frontal eye fields (superior frontal gyrus); FrOperIns_3: the third region of the frontal operculum insula (insula); ns: non-significant. ↓ indicates a significant decrease in MDD; ↑ indicates a significant increase in MDD. * indicates a significant correlation with the HAMD score.

Since the resting brain maintains a dynamic balance between segregation and integration, a higher switch probability between the positive and negative states in the HCs could suggest switch flexibility between network segregation and integration to satisfy the upcoming demands of different cognitive processes (Shine, 2019; Wang et al., 2021). However, such a balance was disrupted in the MDD cohort, indicated by a reduced fractional time and switch frequency to state 4 compared to HCs. This is in line with a previous study indicating reduced segregation of brain functional networks (i.e., clustering coefficient and local efficiency) in an MDD cohort (Yao et al., 2019b). Therefore, we speculate that a lower probability of transitions from positive to negative states of thalamocortical dFC might result in an imbalance between excitatory and inhibitory interactions, e.g., an absence of inhibitory interactions, with consequent cognitive and emotional deficits in MDD patients (Klingner et al., 2014). Other interpretations are possible. For example, the reciprocal glutamatergic excitatory connections between the thalamus and cortex are modulated via inhibitory GABAergic neurons in the thalamic reticular nucleus (Pratt and Morris, 2015). Changes in glutamatergic

and GABAergic signals may interfere with the flow of information between the thalamus and cortex, probably resulting in positive symptoms in MDD patients. This is consistent with growing evidence showing glutamatergic dysfunction in depression and the efficacy of the NMDA receptor antagonist ketamine in treatment-resistant depression (Sanacora et al., 2012). In addition, some electrophysiological studies have shown that an imbalanced excitatory and inhibitory neurotransmitter input to thalamic nuclei can produce hyperpolarized conditions that drive thalamic neurons into a low-frequency burst mode of low-threshold calcium spikes, leading to the thalamocortical dysrhythmia, a common oscillatory mechanism in depression (Llinás et al., 1999, 2005; Steriade, 2001). The abnormal low-frequency oscillations in the thalamocortical circuitry would disrupt perception and sensory integration, and have been proven to play an important role in pain processing (Llinás and Paré, 1991; Groh et al., 2018). Thus, abnormal transitions between thalamocortical dFC states could be regarded as a potential manifestation of thalamocortical dysrhythmia, which may be linked to some common depression symptoms such as headaches and back pain (Vaccarino et al., 2009).

Generally, MDD is characterized by persistent low mood and absence of positive effect accompanied by behavioral and cognitive disturbances (Otte et al., 2016). These symptoms are associated with increased thalamocortical FC. For example, hyper-connectivity connecting the thalamus with the prefrontal, temporal, and somatosensory cortices may be related to the impairments in somatic symptoms, attentional behavior (e.g., negative attentional bias), and self-consciousness (e.g., rumination) in patients with MDD (Brown et al., 2017; Chen et al., 2021; Yu et al., 2021; Zheng et al., 2021). These studies partly support our findings of the decreased occurrence of a negative connectivity state and increased FC dynamics of hyper-connectivity in the MDD group. In addition, more positive connectivity between the thalamus and the higher-order cortices than the visual and somatomotor cortices in the negative connectivity state (state 4) revealed by the analysis of the whole thalamocortical circuit might also indicate an abnormal inhibitory interaction between the thalamus and higher-order cortices 1 in the MDD cohorts (Klingner et al., 2014).

However, dFC analysis that treats the FC between the thalamus and the cortex as a whole system may not be able to capture the specific alterations in the local thalamocortical circuits. Therefore, we performed a thalamo-subnetwork dFC analysis to capture more detailed changes in dFC patterns and found aberrant dFC variability between the thalamus and higher-order cortical networks (i.e., the Default, DorsAttn, and SalVentAttn) in MDD patients. These results suggest that discovering MDD-related dFC abnormalities in the thalamocortical system should not be limited to whole-circuitry analysis and should focus also on local circuits. The FC patterns between thalamic subregions (i.e., the pulvinar, mediodorsal, intralaminar, and ventral lateral nuclei) and higher-order cortical networks (i.e., the Default, DorsAttn, and salience networks) have been reported to be associated with the development of cognitive functions during brain maturation (Steiner et al., 2020). A previous study by Kong et al. (2018) revealed alterations in thalamic FC with the Default network in patients with MDD and suggested that the thalamus-targeted modulation of thalamo-Default connectivity might be an effective method to improve autobiographical memory disturbances in depression. In this study, we showed that MDD patients had aberrant FC dynamics between the thalamus and the Default and DorsAttn networks, with a focus on the frontal and temporal cortices that are implicated in negative emotions and self-related processing (Brown et al., 2017; Chen et al., 2021). This suggests that the altered dFC patterns between multiple thalamic nuclei and higher-order cortical networks may be a potential neural basis of cognitive impairments in the MDD cohort.

Aberrant temporal properties were also detected in the primary local circuits (i.e., the thalamo-Vis and thalamo-SomMot connectivity) of the thalamocortical connectivity system. Specifically, patients with MDD spent less time in the negative connectivity state (state 3 for the thalamo-Vis system and state 2 for the thalamo-SomMot system) and were less inclined to transition from the positive connectivity state (states 1 and 4) to the negative connectivity state (state 3) in the thalamo-Vis system. The visual and somatomotor networks are key components of the perceptual system, which is associated with the processing of external environment information (Liu et al., 2017). Previous rodent studies have suggested that the thalamus delivers orientation- and direction-tuned inputs to layer 4 of the primary visual cortex and regulates the development and manifestation of arousal states in this region

(Sun et al., 2016; Murata and Colonnese, 2018). Moreover, studies of the primary visual and somatosensory cortices provided evidence that response tuning of the layer 4 cells primarily depends on feed-forward excitation from the thalamus and dominant feed-forward inhibition from the interneurons driven by the thalamus (Miller et al., 2001). Thus, the positive and negative connectivities might reflect the excitatory and inhibitory modulation, respectively, of the thalamus to the primary visual/somatosensory cortex. The altered temporal properties within the thalamo-Vis and thalamo-SomMot circuits might indicate an imbalance of excitation-inhibition regulation between the thalamus and primary cortical networks. A previous study showed that altered excitability of the visual cortex might be related to a deficit of visual perception processing (Du et al., 2022). Moreover, the altered intrinsic activity in the somatosensory areas and the hyper-connectivity between the somatosensory cortex and the thalamus may serve as pathophysiological mechanisms of somatic symptoms in depression (Brown et al., 2017; Liu et al., 2021). Therefore, the imbalanced excitation-inhibition regulation between the thalamus and primary cortical networks may be associated with somatic symptoms and impairment of sensory processing in the MDD cohort.

Brain functional lateralization, measured by inter- and intra-hemispheric functional interactions, is beneficial to efficient information processing (Zhu et al., 2018; Güntürkün et al., 2020). The DLI and LF characterize the time-varying asymmetric patterns of inter-hemispherical interactions in the thalamocortical system involved in adaptation to changing environmental demands (Doron et al., 2012; Wu et al., 2022). A higher LF value shows that connectivity switches more frequently between intra- and inter-hemispherical interactions over time, indicating that brain regions are constantly leaving their dominant functional states. This may hamper the cognitive performance of individuals (Wu et al., 2022). In this study, we observed that MDD patients exhibited greater fluctuations of connectivity laterality between the thalamus and the whole cortex, suggesting an atypical inter-hemispheric interaction pattern in the thalamocortical system. Previous studies have reported abnormal hemispheric specialization in MDD, demonstrating that the lateralized and efficient brain information processing system is damaged in patients with MDD (Bruder et al., 2017; Ding et al., 2021). Our results provide further evidence for the disrupted brain lateralization architecture in MDD patients and go a step further by showing that the thalamocortical connectivity within and between hemispheres would vary considerably over time. This is probably related to emotional and cognitive processing deficits in the MDD cohort. Moreover, we observed greater temporal variation in functional laterality of connectivity between the thalamus and higher-order cortical subnetworks (e.g., Cont, DorsAttn, and SalventAttn), suggesting that the hemispheric connectivity patterns would vary at multiple scales in the thalamocortical circuitry. These changes might be associated with potential cognitive deficits, especially in the aspects of attention and memory processing, in depressive patients (Kaiser et al., 2015; Ding et al., 2021).

There were several limitations in this study. First, we did not consider the effect of different antidepressant medications, as the medication information of some participants was missing. It will be important to explore the possible effects of antidepressant medications in future studies. Second, the sample size was relatively small, which may affect the generalization of the results. A replicated study on a large independent dataset is needed to test the reproducibility of this work. Third, we used the AR-DCC model to overcome the issue that conventional methods are largely influenced by the choice of window size. The AR-DCC model is suggested to be less susceptible to noise, but whether the findings are generalizable across different dFC methods (e.g., the coactivation pattern analytical approach (Liu et al., 2018), and the Hidden Markov Model (Chen et al., 2016)) remains unclear. Future studies are warranted to compare the results of different dFC approaches and assess their reproducibility.

5 Conclusions

This is the first study that has comprehensively explored the alterations of dFC patterns in thalamocortical circuitry in patients with MDD. In particular, we have identified heterogeneous changes in dynamic interactions between the thalamus and both primary and higher-order cortical networks that may serve as a potential neural mechanism resulting in the deficits of sensory and cognitive processing in MDD. Our

findings support and extend the evidence for dynamic alteration in patterns of thalamocortical circuitry in MDD cohorts, thereby enhancing our understanding of the essential role played by thalamocortical connectivity in the pathophysiology of depression.

Data availability statement

The data that support our findings are available from the corresponding author upon reasonable request.

Acknowledgments

This work was supported by the Science and Technology Innovation 2030-Major Projects (Nos. 2021ZD0202000, 2021ZD0200800, and 2021ZD0200701), the National Key Research and Development Program of China (No. 2019YFA0706200), the National Natural Science Foundation of China (Nos. 62227807, 62202212, U21A20520, and U22A2033), and the Science and Technology Program of Gansu Province (No. 23YFGA0004), China.

Author contributions

Weihao ZHENG and Qin ZHANG designed the draft of the research process and prepared the manuscript. Qin ZHANG performed the experiments and statistical analyses. Weihao ZHENG, Ziyang ZHAO, Pengfei ZHANG, Leilei ZHAO, Xiaomin WANG, and Songyu YANG guided the experiments. Jing ZHANG guided the experiment and revised the manuscript. Weihao ZHENG, Zhijun YAO, and Bin HU provided funding for the experiment. All authors contributed to the interpretation and review of the manuscript. All authors have read and approved the final manuscript, and therefore, have full access to all the data in the study and take responsibility for the integrity and security of the data.

Compliance with ethics guidelines

Weihao ZHENG, Qin ZHANG, Ziyang ZHAO, Pengfei ZHANG, Leilei ZHAO, Xiaomin WANG, Songyu YANG, Jing ZHANG, Zhijun YAO, and Bin HU declare that they have no conflict of interest.

All procedures followed were in accordance with the ethical standards of the responsible committee on human experimentation (institutional and national) and with the Helsinki Declaration of 1975, as revised in 2013. This study was approved by the Ethics Committee of the Gansu Provincial Hospital (No. 2017-071). All participants provided written informed consent before scanning.

References

Aggarwal CC, Hinneburg A, Keim DA, 2001. On the surprising behavior of distance metrics in high dimensional space. Database Theory—ICDT 2001, Berlin, Heidelberg. Springer Berlin Heidelberg, p.420-434. https://doi.org/10.1007/3-540-44503-X_27

Allen EA, Damaraju E, Plis SM, et al., 2014. Tracking whole-brain connectivity dynamics in the resting state. *Cereb Cortex*, 24(3):663-676. https://doi.org/10.1093/cercor/bhs352

Arbabshirani MR, Damaraju E, Phlypo R, et al., 2014. Impact of autocorrelation on functional connectivity. *NeuroImage*, 102(Part 2):294-308. https://doi.org/10.1016/j.neuroimage.2014.07.045

Avants B, Tustison NJ, Song G, 2009. Advanced Normalization Tools: V1.0. *Insight J*, July-December. https://doi.org/10.54294/uvnhin

Behrens TEJ, Johansen-Berg H, Woolrich MW, et al., 2003. Non-invasive mapping of connections between human thalamus and cortex using diffusion imaging. *Nat Neurosci*, 6(7):750-757. https://doi.org/10.1038/nn1075

Bos DJ, Oranje B, Achterberg M, et al., 2017. Structural and functional connectivity in children and adolescents with and without attention deficit/hyperactivity disorder. *J Child Psychol Psychiatry*, 58(7):810-818. https://doi.org/10.1111/jcpp.12712

Brown EC, Clark DL, Hassel S, et al., 2017. Thalamocortical connectivity in major depressive disorder. *J Affect Disord*, 217:125-131. https://doi.org/10.1016/j.jad.2017.04.004

Bruder GE, Stewart JW, McGrath PJ, 2017. Right brain, left brain in depressive disorders: clinical and theoretical implications of behavioral, electrophysiological and neuroimaging findings. *Neurosci Biobehav Rev*, 78:178-191. https://doi.org/10.1016/j.neubiorev.2017.04.021

Calhoun VD, Miller R, Pearlson G, et al., 2014. The chronnectome: time-varying connectivity networks as the next frontier in fMRI data discovery. *Neuron*, 84(2):262-274. https://doi.org/10.1016/j.neuron.2014.10.015

Chen FF, Lv XY, Fang JL, et al., 2021. Body-mind relaxation meditation modulates the thalamocortical functional connectivity in major depressive disorder: a preliminary resting-state fMRI study. *Transl Psychiatry*, 11:546. https://doi.org/10.1038/s41398-021-01637-8

Chen QL, Beaty RE, Cui ZX, et al., 2019. Brain hemispheric involvement in visuospatial and verbal divergent thinking. *NeuroImage*, 202:116065. https://doi.org/10.1016/j.neuroimage.2019.116065

Chen SY, Langley J, Chen XC, et al., 2016. Spatiotemporal modeling of brain dynamics using resting-state functional magnetic resonance imaging with Gaussian Hidden Markov model. *Brain Connect*, 6(4):326-334. https://doi.org/10.1089/brain.2015.0398

Choe AS, Nebel MB, Barber AD, et al., 2017. Comparing test-retest reliability of dynamic functional connectivity methods. *NeuroImage*, 158:155-175. https://doi.org/10.1016/j.neuroimage.2017.07.005

Choi J, Jeong B, Lee SW, et al., 2013. Aberrant development of functional connectivity among resting state-related functional networks in medication-naive ADHD children. *PLoS ONE*, 8(12):e83516. https://doi.org/10.1371/journal.pone.0083516

Ding YD, Yang R, Yan CG, et al., 2021. Disrupted hemispheric

connectivity specialization in patients with major depressive disorder: evidence from the REST-meta-MDD Project. *J Affect Disord*, 284:217-228. https://doi.org/10.1016/j.jad.2021.02.030

Doron KW, Bassett DS, Gazzaniga MS, 2012. Dynamic network structure of interhemispheric coordination. *Proc Natl Acad Sci USA*, 109(46):18661-18668. https://doi.org/10.1073/pnas.1216402109

Du HH, Shen X, Du XY, et al., 2022. Altered visual cortical excitability is associated with psychopathological symptoms in major depressive disorder. *Front Psychiatry*, 13: 844434. https://doi.org/10.3389/fpsyt.2022.844434

Dupire A, Kant P, Mons N, et al., 2013. A role for anterior thalamic nuclei in affective cognition: interaction with environmental conditions. *Hippocampus*, 23(5):392-404. https://doi.org/10.1002/hipo.22098

Fischl B, 2012. FreeSurfer. *NeuroImage*, 62(2):774-781. https://doi.org/10.1016/j.neuroimage.2012.01.021

Fox MD, Snyder AZ, Vincent JL, et al., 2005. The human brain is intrinsically organized into dynamic, anticorrelated functional networks. *Proc Natl Acad Sci USA*, 102(27): 9673-9678. https://doi.org/10.1073/pnas.0504136102

Fox MD, Zhang DY, Snyder AZ, et al., 2009. The global signal and observed anticorrelated resting state brain networks. *J Neurophysiol*, 101(6):3270-3283. https://doi.org/10.1152/jn.90777.2008

Gotlib IH, Jonides J, Buschkuehl M, et al., 2011. Memory for affectively valenced and neutral stimuli in depression: evidence from a novel matching task. *Cognit Emotion*, 25(7): 1246-1254. https://doi.org/10.1080/02699931.2010.538374

Groh A, Krieger P, Mease RA, et al., 2018. Acute and chronic pain processing in the thalamocortical system of humans and animal models. *Neuroscience*, 387:58-71. https://doi.org/10.1016/j.neuroscience.2017.09.042

Güntürkün O, Ströckens F, Ocklenburg S, 2020. Brain lateralization: a comparative perspective. *Physiol Rev*, 100(3): 1019-1063. https://doi.org/10.1152/physrev.00006.2019

Hakimdavoodi H, Amirmazlaghani M, 2020. Using autoregressive-dynamic conditional correlation model with residual analysis to extract dynamic functional connectivity. *J Neural Eng*, 17(3):035008. https://doi.org/10.1088/1741-2552/ab965b

Hamilton JP, Chen MC, Waugh CE, et al., 2015. Distinctive and common neural underpinnings of major depression, social anxiety, and their comorbidity. *Soc Cogn Affect Neurosci*, 10(4):552-560. https://doi.org/10.1093/scan/nsu084

Hamilton M, 1967. Development of a rating scale for primary depressive illness. *Br J Soc Clin Psychol*, 6(4):278-296. https://doi.org/10.1111/j.2044-8260.1967.tb00530.x

Hutchison RM, Womelsdorf T, Gati JS, et al., 2013. Resting-state networks show dynamic functional connectivity in awake humans and anesthetized macaques. *Hum Brain Mapp*, 34(9):2154-2177. https://doi.org/10.1002/hbm.22058

Iglesias JE, Insausti R, Lerma-Usabiaga G, et al., 2018. A probabilistic atlas of the human thalamic nuclei combining *ex vivo* MRI and histology. *NeuroImage*, 183:314-326. https://doi.org/10.1016/j.neuroimage.2018.08.012

Kaiser RH, Andrews-Hanna JR, Wager TD, et al., 2015. Large-scale network dysfunction in major depressive disorder: a meta-analysis of resting-state functional connectivity. *JAMA Psychiatry*, 72(6):603-611. https://doi.org/10.1001/jamapsychiatry.2015.0071

Kang LJ, Zhang AX, Sun N, et al., 2018. Functional connectivity between the thalamus and the primary somatosensory cortex in major depressive disorder: a resting-state fMRI study. *BMC Psychiatry*, 18:339. https://doi.org/10.1186/s12888-018-1913-6

Klingner CM, Langbein K, Dietzek M, et al., 2014. Thalamocortical connectivity during resting state in schizophrenia. *Eur Arch Psychiatry Clin Neurosci*, 264(2):111-119. https://doi.org/10.1007/s00406-013-0417-0

Kong QM, Qiao H, Liu CZ, et al., 2018. Aberrant intrinsic functional connectivity in thalamo-cortical networks in major depressive disorder. *CNS Neurosci Ther*, 24(11): 1063-1072. https://doi.org/10.1111/cns.12831

Lenoski B, Baxter LC, Karam LJ, et al., 2008. On the performance of autocorrelation estimation algorithms for fMRI analysis. *IEEE J Sel Top Signal Process*, 2(6):828-838. https://doi.org/10.1109/JSTSP.2008.2007819

Lindquist MA, Xu YT, Nebel MB, et al., 2014. Evaluating dynamic bivariate correlations in resting-state fMRI: a comparison study and a new approach. *NeuroImage*, 101: 531-546. https://doi.org/10.1016/j.neuroimage.2014.06.052

Liu F, Wang YF, Li ML, et al., 2017. Dynamic functional network connectivity in idiopathic generalized epilepsy with generalized tonic-clonic seizure. *Hum Brain Mapp*, 38(2): 957-973. https://doi.org/10.1002/hbm.23430

Liu PH, Tu HW, Zhang AX, et al., 2021. Brain functional alterations in MDD patients with somatic symptoms: a resting-state fMRI study. *J Affect Disord*, 295:788-796. https://doi.org/10.1016/j.jad.2021.08.143

Liu X, Zhang NY, Chang C, et al., 2018. Co-activation patterns in resting-state fMRI signals. *NeuroImage*, 180:485-494. https://doi.org/10.1016/j.neuroimage.2018.01.041

Llinás RR, Paré D, 1991. Of dreaming and wakefulness. *Neuroscience*, 44(3):521-535. https://doi.org/10.1016/0306-4522(91)90075-Y

Llinás RR, Ribary U, Jeanmonod D, et al., 1999. Thalamocortical dysrhythmia: a neurological and neuropsychiatric syndrome characterized by magnetoencephalography. *Proc Natl Acad Sci USA*, 96(26):15222-15227. https://doi.org/10.1073/pnas.96.26.15222

Llinás RR, Urbano FJ, Leznik E, et al., 2005. Rhythmic and dysrhythmic thalamocortical dynamics: GABA systems and the edge effect. *Trends Neurosci*, 28(6):325-333. https://doi.org/10.1016/j.tins.2005.04.006

Long YC, Cao HY, Yan CG, et al., 2020. Altered resting-state

dynamic functional brain networks in major depressive disorder: findings from the REST-meta-MDD consortium. *NeuroImage Clin*, 26:102163. https://doi.org/10.1016/j.nicl.2020.102163

Lu FM, Chen YC, Cui Q, et al., 2023. Shared and distinct patterns of dynamic functional connectivity variability of thalamo-cortical circuit in bipolar depression and major depressive disorder. *Cereb Cortex*, 33(11):6681-6692. https://doi.org/10.1093/cercor/bhac534

Lui S, Wu QZ, Qiu LH, et al., 2011. Resting-state functional connectivity in treatment-resistant depression. *Am J Psychiatry*, 168(6):642-648. https://doi.org/10.1176/appi.ajp.2010.10101419

Lund TE, Madsen KH, Sidaros K, et al., 2006. Non-white noise in fMRI: does modelling have an impact? *NeuroImage*, 29(1):54-66. https://doi.org/10.1016/j.neuroimage.2005.07.005

McLeod KR, Langevin LM, Goodyear BG, et al., 2014. Functional connectivity of neural motor networks is disrupted in children with developmental coordination disorder and attention-deficit/hyperactivity disorder. *NeuroImage Clin*, 4:566-575. https://doi.org/10.1016/j.nicl.2014.03.010

Miller KD, Pinto DJ, Simons DJ, 2001. Processing in layer 4 of the neocortical circuit: new insights from visual and somatosensory cortex. *Curr Opin Neurobiol*, 11(4):488-497. https://doi.org/10.1016/S0959-4388(00)00239-7

Murata Y, Colonnese MT, 2018. Thalamus controls development and expression of arousal states in visual cortex. *J Neurosci*, 38(41):8772-8786. https://doi.org/10.1523/JNEUROSCI.1519-18.2018

Otte C, Gold SM, Penninx BW, et al., 2016. Major depressive disorder. *Nat Rev Dis Primers*, 2:16065. https://doi.org/10.1038/nrdp.2016.65

Pratt JA, Morris BJ, 2015. The thalamic reticular nucleus: a functional hub for thalamocortical network dysfunction in schizophrenia and a target for drug discovery. *J Psychopharmacol*, 29(2):127-137. https://doi.org/10.1177/0269881114565805

Purdon PL, Weisskoff RM, 1998. Effect of temporal autocorrelation due to physiological noise and stimulus paradigm on voxel-level false-positive rates in fMRI. *Hum Brain Mapp*, 6(4):239-249. https://doi.org/10.1002/(SICI)1097-0193(1998)6:4<239::AID-HBM4>3.0.CO;2-4

Rosen AFG, Roalf DR, Ruparel K, et al., 2018. Quantitative assessment of structural image quality. *NeuroImage*, 169:407-418. https://doi.org/10.1016/j.neuroimage.2017.12.059

Saalmann YB, 2014. Intralaminar and medial thalamic influence on cortical synchrony, information transmission and cognition. *Front Syst Neurosci*, 8:83. https://doi.org/10.3389/fnsys.2014.00083

Sacchet MD, Ho TC, Connolly CG, et al., 2016. Large-scale hypoconnectivity between resting-state functional networks in unmedicated adolescent major depressive disorder. *Neuropsychopharmacology*, 41(12):2951-2960. https://doi.org/10.1038/npp.2016.76

Sanacora G, Treccani G, Popoli M, 2012. Towards a glutamate hypothesis of depression: an emerging frontier of neuropsychopharmacology for mood disorders. *Neuropharmacology*, 62(1):63-77. https://doi.org/10.1016/j.neuropharm.2011.07.036

Schaefer A, Kong R, Gordon EM, et al., 2018. Local-global parcellation of the human cerebral cortex from intrinsic functional connectivity MRI. *Cereb Cortex*, 28(9):3095-3114. https://doi.org/10.1093/cercor/bhx179

Sendi MSE, Zendehrouh E, Sui J, et al., 2021. Abnormal dynamic functional network connectivity estimated from default mode network predicts symptom severity in major depressive disorder. *Brain Connect*, 11(10):838-849. https://doi.org/10.1089/brain.2020.0748

Sherman SM, 2007. The thalamus is more than just a relay. *Curr Opin Neurobiol*, 17(4):417-422. https://doi.org/10.1016/j.conb.2007.07.003

Shine JM, 2019. Neuromodulatory influences on integration and segregation in the brain. *Trends Cogn Sci*, 23(7):572-583. https://doi.org/10.1016/j.tics.2019.04.002

Steiner L, Federspiel A, Slavova N, et al., 2020. Functional topography of the thalamo-cortical system during development and its relation to cognition. *NeuroImage*, 223:117361. https://doi.org/10.1016/j.neuroimage.2020.117361

Steriade M, 2001. Impact of network activities on neuronal properties in corticothalamic systems. *J Neurophysiol*, 86(1):1-39. https://doi.org/10.1152/jn.2001.86.1.1

Sun WZ, Tan ZC, Mensh BD, et al., 2016. Thalamus provides layer 4 of primary visual cortex with orientation- and direction-tuned inputs. *Nat Neurosci*, 19(2):308-315. https://doi.org/10.1038/nn.4196

Sweeney-Reed CM, Buentjen L, Voges J, et al., 2021. The role of the anterior nuclei of the thalamus in human memory processing. *Neurosci Biobehav Rev*, 126:146-158. https://doi.org/10.1016/j.neubiorev.2021.02.046

Tadayonnejad R, Yang SL, Kumar A, et al., 2015. Clinical, cognitive, and functional connectivity correlations of resting-state intrinsic brain activity alterations in unmedicated depression. *J Affect Disord*, 172:241-250. https://doi.org/10.1016/j.jad.2014.10.017

Vaccarino AL, Sills TL, Evans KR, et al., 2009. Multiple pain complaints in patients with major depressive disorder. *Psychosom Med*, 71(2):159-162. https://doi.org/10.1097/psy.0b013e3181906572

Wang R, Liu MX, Cheng XH, et al., 2021. Segregation, integration, and balance of large-scale resting brain networks configure different cognitive abilities. *Proc Natl Acad Sci USA*, 118(23):e2022288118. https://doi.org/10.1073/pnas.2022288118

Weeland CJ, Vriend C, van der Werf Y, et al., 2022a. Thalamic subregions and obsessive-compulsive symptoms in 2,500 children from the general population. *J Am Acad Child Adolesc Psychiatry*, 61(2):321-330.

https://doi.org/10.1016/j.jaac.2021.05.024

Weeland CJ, Kasprzak S, de Joode NT, et al., 2022b. The thalamus and its subnuclei—a gateway to obsessive-compulsive disorder. *Transl Psychiatry*, 12:70. https://doi.org/10.1038/s41398-022-01823-2

Wei Q, Bai TJ, Brown EC, et al., 2020. Thalamocortical connectivity in electroconvulsive therapy for major depressive disorder. *J Affect Disord*, 264:163-171. https://doi.org/10.1016/j.jad.2019.11.120

Williams JBW, 1988. A structured interview guide for the Hamilton Depression Rating Scale. *Arch Gen Psychiatry*, 45(8):742-747. https://doi.org/10.1001/archpsyc.1988.01800320058007

Wu XR, Kong XZ, Vatansever D, et al., 2022. Dynamic changes in brain lateralization correlate with human cognitive performance. *PLoS Biol*, 20(3):e3001560. https://doi.org/10.1371/journal.pbio.3001560

Xue SW, Wang D, Tan Z, et al., 2019. Disrupted brain entropy and functional connectivity patterns of thalamic subregions in major depressive disorder. *Neuropsychiatr Dis Treat*, 15:2629-2638. https://doi.org/10.2147/ndt.s220743

Yan CG, Zang YF, 2010. DPARSF: a MATLAB toolbox for "pipeline" data analysis of resting-state fMRI. *Front Syst Neurosci*, 4:13. https://doi.org/10.3389/fnsys.2010.00013

Yao ZJ, Shi J, Zhang Z, et al., 2019a. Altered dynamic functional connectivity in weakly-connected state in major depressive disorder. *Clin Neurophysiol*, 130(11):2096-2104. https://doi.org/10.1016/j.clinph.2019.08.009

Yao ZJ, Zou Y, Zheng WH, et al., 2019b. Structural alterations of the brain preceded functional alterations in major depressive disorder patients: evidence from multimodal connectivity. *J Affect Disord*, 253:107-117. https://doi.org/10.1016/j.jad.2019.04.064

Yu YM, Zheng WH, Tan XF, et al., 2021. Microstructural profiles of thalamus and thalamocortical connectivity in patients with disorder of consciousness. *J Neurosci Res*, 99(12):3261-3273. https://doi.org/10.1002/jnr.24921

Yuan R, Di X, Taylor PA, et al., 2016. Functional topography of the thalamocortical system in human. *Brain Struct Funct*, 221(4):1971-1984. https://doi.org/10.1007/s00429-015-1018-7

Zhang DY, Snyder AZ, Shimony JS, et al., 2010. Noninvasive functional and structural connectivity mapping of the human thalamocortical system. *Cereb Cortex*, 20(5):1187-1194. https://doi.org/10.1093/cercor/bhp182

Zhao ZY, Zhang YH, Chen N, et al., 2022. Altered temporal reachability highlights the role of sensory perception systems in major depressive disorder. *Prog Neuropsychopharmacol Biol Psychiatry*, 112:110426. https://doi.org/10.1016/j.pnpbp.2021.110426

Zheng WH, Tan XF, Liu TT, et al., 2021. Individualized thalamic parcellation reveals alterations in shape and microstructure of thalamic nuclei in patients with disorder of consciousness. *Cereb Cortex Commun*, 2(2):tgab024. https://doi.org/10.1093/texcom/tgab024

Zhi DM, Calhoun VD, Lv LX, et al., 2018. Aberrant dynamic functional network connectivity and graph properties in major depressive disorder. *Front Psychiatry*, 9:339. https://doi.org/10.3389/fpsyt.2018.00339

Zhu FR, Liu F, Guo WB, et al., 2018. Disrupted asymmetry of inter- and intra-hemispheric functional connectivity in patients with drug-naive, first-episode schizophrenia and their unaffected siblings. *eBioMedicine*, 36:429-435. https://doi.org/10.1016/j.ebiom.2018.09.012

Supplementary information

Tables S1–S3; Figs. S1–S8